Journal name
000(00):1–13

DOI:doi number
http://mms.sagepub.com

A study of the effect of projectile orientation on the results of ballistic impact tests as described in the EASA CS-25 regulations for fuel tank access covers

T. De Vuyst*
Structural Integrity - Dynamic Response, Brunel University London, NSIRC, Granta Park, Great Abington, Cambridgshire, CB21 6AL, UK

R. Vignjevic
Structural Integrity - Dynamic Response, Brunel University London, Uxbridge

A. Azorin Albero
Applied Mechanics, Cranfield University, UK

J.C. Campbell
Structural Integrity - Dynamic Response, Brunel University London

N. Djordjevic
Structural Integrity - Dynamic Response, Brunel University London

K. Hughes
Structural Integrity - Dynamic Response, Brunel University London

Abstract

This paper presents the results of an investigation of the ballistic limits and failure modes of AA2024-T351 sheets impacted cubical projectiles. The experiment/test setup was based on EASA CS-25 regulations for fuel tank access covers. The effect of cube orientation on the ballistic limit and failure modes was considered in detail. A 25% variation in ballistic limit was observed with the lowest ballistic limit ($202 m/s$) observed for the cubical projectile edge impacted on the target. In the

* Corresponding author; e-mail: tom.devuyst@brunel.ac.uk

cube face impacts the ballistic limit was higher ($223m/s$), and the highest ballistic limit ($254m/s$) was observed for the corner impact. The observed differences in the ballistic limit were due to differences in failure mechanism which resulted in different localised deformation near the projectile impact point but also led to differences in global, dishing, deformation.

Keywords
EASA CS-25, fuel tank access cover, ballistic impact, cube projectiles, engine debris

1. Introduction

In the literature on ballistic limit studies the many publications considered cylindrical (rod-shaped) projectiles with a range of nose shapes, and the most common types of nose shapes are ogive, flat, conical and hemispherical. Authors such as Gupta et. al.[1,2] studied the ballistic performance of thin AA1100 plates impacted by cylindrical projectiles with different nose shapes. Other authors such as Rusinek et al.[3–6] and Børvik et al.[7] have also studied the effect of the nose shape of cylindrical projectiles on the ballistic limit of various target configurations. The work referred to above studied rod shaped impactors, however other authors consider impactors with an aspect ratio close to one, sometimes labelled compact fragments. For example, Erice et al.[8] considers the impact of $5.55mm$ diameter steel spherical projectiles on $1.6mm$ thick Inconel 718 plates, and Jordan[9] studies a range of compact fragment geometries impacting on GFRP sheets with thicknesses of 4, 9, $14mm$. Ulven et al.[10] studied hemispherical, flat and conical nosed cylindrical projectiles with aspect ratio close to one but the targets used in this research are carbon/epoxy laminates of 6.5 and $3.2mm$ thickness. A similar study was performed by Tan et al.[11] who consider sheet targets made of aramid fibre fabric. Wang and Zhou[12] study the penetration of $5mm$ thick explosively welded steel/aluminium plates when subjected to impacts by cylindrical (diameter $6mm$) and cubical (length $4.2mm$) projectiles. The cube impacts the target face-on. The ballistic limit was lower for the spherical projectile. Apart from these generic studies there have been a number of publications specifically looking into the effect debris impact on aircraft. The work by Wang[13] was performed within the context of Foreign Object Damage (FOD) and consists of numerical modelling results of spherical projectiles impacting $3.175mm$ thick Ti Al6 4V sheets. This work does not consider penetration only the impact crater shape on the target. An FAA report report by Buyuk et al.[14] studied the impact of spherical, cylindrical and prismatic projectiles on AA2024-T351 sheets of thickness $1.588mm$, $3.175mm$, $6.350mm$. The focus of the work was on evaluating the ability of Johnson Cook model to predict ballistic limit. Tests were performed with $12.7mm$ diameter steel sphere on 305x305mm square plates. The failure modes transitioned from mainly dishing and petalling for low thickness plates towards plugging for higher thickness plates. The ballistic limit for $3.175mm$ plate is about $210m/s$. These authors predict a ballistic limit for face impact of a cube to be higher than for sphere. Other FAA reports, by Kelly and Johnson[15] and Kay et al.[16], were produced within the context of airplane rotor burst fragment shielding. These reports describe impact test results on AA2024-T351 sheets impacted by $12.7mm$ spherical projectiles and $12.7mm$ diameter rods. Ti-6Al-4V, polycarbonate and composite panels are also tested. The problem of debris impact on fuel tank covers was studied by Ryabov et al.[17], but the debris considered was a large tyre debris fragment, not a hard and compact metallic debris fragment. In terms of studying projectile orientation a paper by Williamsen et al.[18] did consider cube orientation (edge, face and corner impact) but within the context of hypervelocity impact, and the lowest velocity that was considered is $500m/s$. The target considered was a Whipple shield. The FATEPEN model used to predict ballistic limit for normal impact predicts a ballistic limit of cube projectiles that is higher than that for a sphere of the same characteristic length. From the review of relevant literature above it can be observed that the impact of cube shaped projectiles has received relatively little attention. The impact of cubical projectiles is of relevance to the certification of aircraft fuel tanks as defined in EASA CS-25 regulations[19] and Aircraft Engine Containment and Fragment Shielding, as studied in FAA reports[15,16]. More specifically the EASA CS-25 regulations require that fuel tank access covers should be evaluated for impact resistance to tyre and engine debris. In the case of engine debris the regulations state that:

In the absence of relevant data, an energy level corresponding to the impact of a 9.5mm (3/8 inch) cube steel debris at 213.4m/s (700fps), 90 degrees to the impacted surface or area should be used.

The objective of the work presented in this paper was to investigate, for the case of cubical projectiles, the effect of projectile orientation on the ballistic limit. In order to achieve this, a number of ballistic impact experiments with cubical projectiles were performed. The cube impact tests were performed for three different cube orientations leading to three impact cases: face, edge and corner as shown in Figure 1. The observed differences in ballistic limit are explained in terms of differences in failure mode for the different impact cases.

2. Experiments Description

The effect of projectile orientation on ballistic limit was determined with a series of impact tests which, similarly to previous work[10,12,14], were performed on 3.175mm thick AA2024-T351 sheets. In line with the fuel tank access cover impact test requirement in EASA CS-25[19] cubical projectiles with an edge length of 9.5mm and mass of 6.9g were used. Three different cube orientations were tested: face, edge and corner impact as shown in Figure 2. The target plates were manufactured from 3.175mm AA2024-T351 and were clamped at two opposite edges, leaving the other two edges free. The unclamped area of the targets was 120mm x 120mm. The experiments were performed with a single stage gas gun using high pressure nitrogen to accelerate the projectiles. The barrel used had a length of 2m and inner diameter of 31mm. At maximum pressure this allowed projectiles to be accelerated to velocities of around 325m/s. The cube orientation was set by mounting each projectile in the correct orientation within the sabot and by minimising the distance between the sabot stripper and the target (about 50mm). Each experiment was recorded by a high-speed video camera, allowing the orientation of the cube to be checked prior to impact. The recordings showed that the desired cube orientation was achieved to an accuracy of approximately $\pm$7 degrees across all the experiments. No rotation of the cube prior to impact was visible in the high speed video for any of the experiments.

3. Results and Discussion

3.1. Experimental Results Overview

The resulting impact and residual velocities are summarised in Table 1 and a plot of residual velocity versus impact velocity is shown in Figure 3. The ballistic limit was calculated by adjusting the parameters a and p of a Recht-Ipson[20] equation to the experimental data.

$$v_r = a\,(v_i^p - v_{bl}^p)^{1/p} \tag{1}$$

where

$$a = \frac{m_{projectile}}{m_{projectile} + m_{plug}} \tag{2}$$

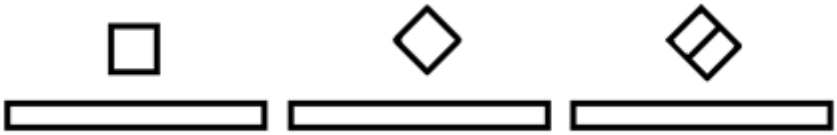

Fig. 1. Impact cases: a) cube face, b) cube edge, c) cube corner

Table 1: Summary of impact and residual velocities for experiments and Recht-Ipson equation

Projectile	v_i $[m/s]$	v_r exp $[m/s]$	v_r analyt $[m/s]$
Face	221	0	0
Face	226	72	71
Face	240	144	111
Face	279	184	122
Face	321	251	155
Edge	198	0	0
Edge	215	47	54
Edge	231	100	88
Edge	272	155	153
Edge	303	189	196
Corner	249	0	0
Corner	263	47	48
Corner	290	111	110
Corner	324	167	168

Table 2: Summary of parameters for the Recht-Ipson equation

Type	Ballistic Limit $[m/s]$	p	a
Face	223	3.0	0.9
Edge	202	1.6	1.0
Corner	254	1.7	1.0

The parameters v_{bl} (the ballistic limit) and parameter p were varied to minimise the RMS error between experimental data and the values predicted by the analytical model, the resulting curves are shown with the experimental data points in Figure 3, the parameters are listed in Table 2. The lowest ballistic limit was observed for the cube edge impact at an impact velocity of $202m/s$. The highest ballistic limit was observed for the cube corner impact at an impact velocity of $254m/s$. The ballistic limit for the cube face impact was $223m/s$. In other words there is a 25% variation in ballistic limit depending on the orientation of a cube shaped projectile.

Figure 3 shows the projectile kinetic energy loss as a function of impact velocity. The points with hollow markers are associated with impacts below the ballistic limit. This figure shows that for the velocity range studied, the energy loss increased with impact velocity for the edge, sphere and corner impacts. The face impact case was different. In the case of a face impact below the ballistic limit, the energy loss of the projectile was higher than for the edge impact at the same velocity. However once the ballistic limit was reached, the face impact resulted in lower projectile energy loss than the corresponding edge impact.

In the next sections each impact case will be described in more detail in terms of the penetration mechanism and the resulting local and global (dishing) deformations.

3.2. Penetration Mechanism

Edge The edge impact configuration is the configuration which resulted in the lowest ballistic limit. For the edge impacts the penetration mechanism consisted of rapid localised deformation around the corner contact area, and as deformation in this area increased ductile fracture occurred in the vicinity, see Figure 4a. Two petals were then formed by the initial

fracture propagating to form an I-shaped crack as shown on the high speed images in Figure 4b. No plug formation was observed in this impact configuration.

Face The failure mode for the face impact configuration was mainly plugging as shown in the high speed pictures in Figure 4c and 4d. Some global bending or dishing was also observed. The impacts below the ballistic limit showed the highest amount of dishing.

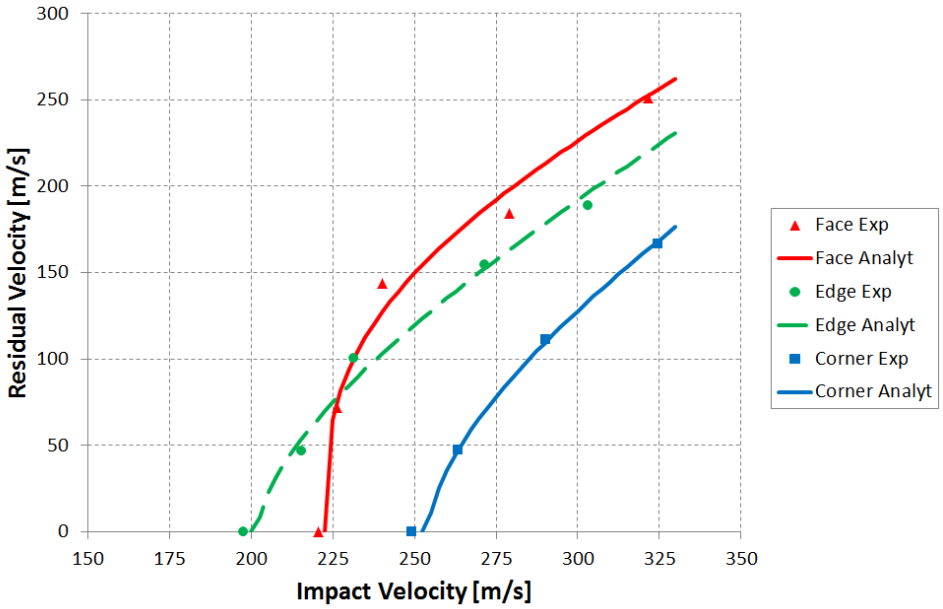

Fig. 2. Ballistic limit curve and Recht-Ipson equation

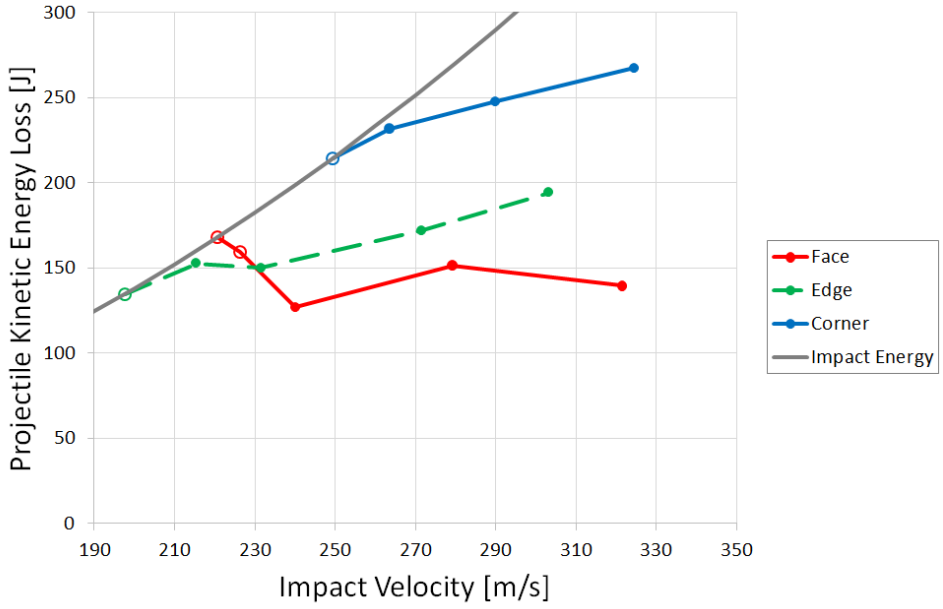

Fig. 3. Kinetic energy loss of the projectile versus impact velocity

Corner In the case of the corner impact the failure mechanism is similar to the edge impact. First cracks appear through tensile failure near the impact point. In this case this results in a small triangular fragment which can be seen in Figure 4e. From this initial perforation three cracks (corresponding to the edges which intersect at the impact corner) then propagate.

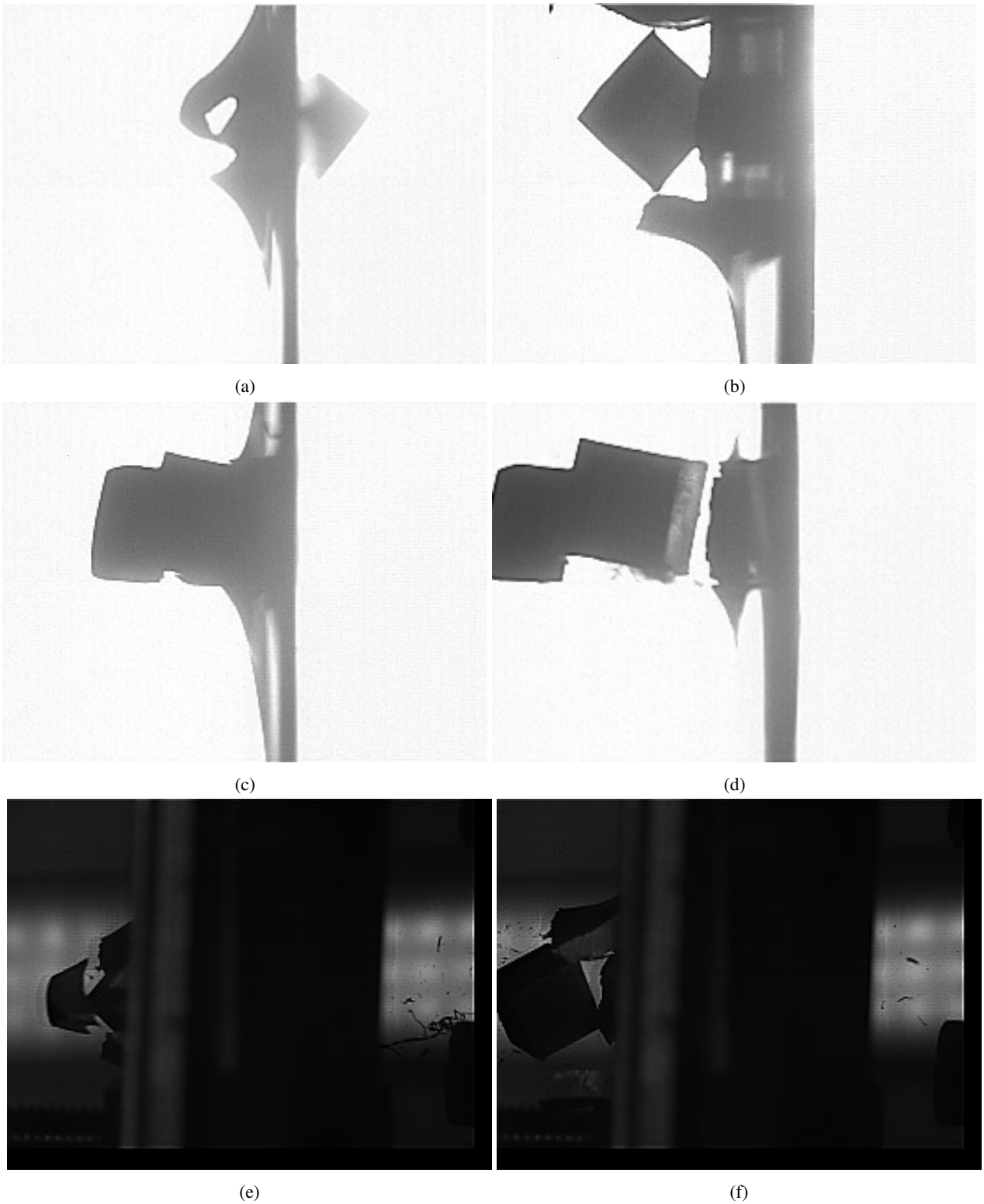

Fig. 4. High speed camera images of a) and b) edge impact, c) and d) face impact, e) and f) corner impact

This results in the formation of three petals. As the projectile advances these petals bend and become larger, in some cases breaking off.

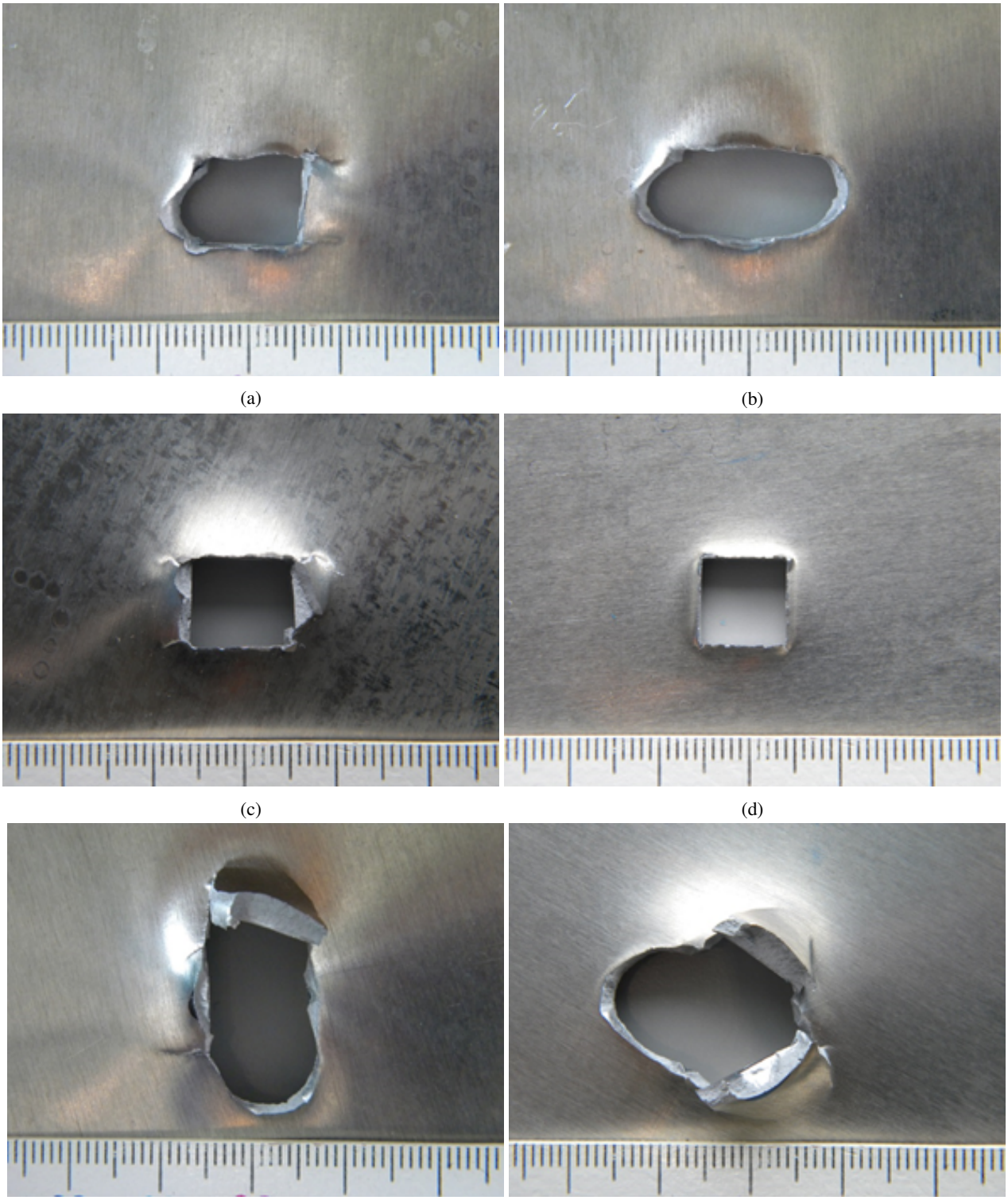

(a) (b)

(c) (d)

(e) (f)

Fig. 5. Deformed state after edge impact at a) $215 m/s$ and b) $303 m/s$, face impact at c) $226 m/s$ and d) $321 m/s$ and corner impact at e) $264 m/s$ and f) $325 m/s$

3.3. Localised Deformation

Edge As the impact velocity increases these petals bend so far that one or both of the petals break off (see Figure 5a and 5b, leaving an elliptical shaped hole. For the $215m/s$ impact one of the petals broke off (see Figure 5a) and the dimensions of the principal axes of the hole are 9.7 and $13.8mm$. In the case of the $303m/s$ impact both petals break off (see Figure 5b) and the dimension of the principal axes are 9.9 and $21.7mm$. The evolution of the size of the hole in the two directions as a function of impact velocity is shown in Figure 6a.

Face In Figure 5c and 5d the deformed state for impact velocities of $226m/s$ and $321m/s$ are shown. The impact velocity of $226m/s$ is the lowest impact velocity resulting in penetration, while the impact velocity of $321m/s$ is the highest tested. The dimension of the hole was relatively unaffected over the velocity range tested, varying from 9.6X9.6mm for the $226m/s$ impact to 9.8X9.8mm for the $321m/s$ impact. In Figure 6b it can be seen that the size of the hole is independent of the impact velocity.

Corner For this failure mode it was not straightforward to define a good measure for the size of the hole in the plate. Measuring hole in the direction perpendicular to the clamped edges and the direction perpendicular to it results in hole dimensions of roughly $15mm$, with lower and upper bounds of 10 and $20mm$. When the hole dimensions are plot as a function of impact velocity (see Figure 6c) then the scatter in the data is apparent. This is due to the variation in petal size and whether they break off or not.

3.4. Dishing and Energy Absorption

Edge It can be seen in Figure 7a that the level of dishing deceased with increasing impact speed. Since overall the energy absorbed increases with impact velocity, as can be seen in Figure 3, this implies that the increase in energy absorbed by the increasing level of bending and breaking of petals with increasing impact velocity is higher than the reduction in energy absorbed by dishing.

Face In comparison with the edge impact there is significantly less dishing of the target except for the impact test at $221m/s$ which did not result in penetration and shows similar levels of dishing as the corresponding edge impact (see Figure 7a and 7b). The level of dishing also decreases with increasing impact speed. Since the level of local deformation also shows little dependence on the impact speed this explains why the energy loss of the projectile (see Figure 3) does not depend on the impact velocity.

Corner The dishing of the plate, see Figure 7c, is higher than in the other impact configurations. The amount of dishing decreases with increasing impact speed (see Figure 7c). The deflection at $264m/s$ is $4.6mm$ and at $325m/s$ $4.4mm$. Since the amount of dishing does not change significantly, the increase in energy absorbed with increasing velocity (see Figure 3) is due to more energy being absorbed in local deformation.

4. Conclusion

In this paper the response of $3.175mm$ thick AA2024-T351 sheets for three cube impact configurations was determined through a series of impact experiments. The results show that the orientation of a cube shaped projectile has a significant effect on the ballistic limit of a $3.175mm$ thick AA2024-T351 sheet. The lowest ballistic limit ($202m/s$) was observed for an edge on impact, while the highest ballistic limit was observed for a corner impact ($254m/s$), ie. a difference of 25%. A face impact results in a ballistic limit of $223m/s$. The reason for this difference is due to the different failure mechanisms. Since the 25% difference in ballistic limit velocity is significant and the test configuration is based on the EASA regulations

for the impact resistance of fuel access covers it can also be concluded that these experiments need to be conducted with sufficient control over the projectile orientation if meaningful comparisons are to be made.

5. Acknowledgement

Tom De Vuyst would like to acknowledge Jarryd Braithwaite for his help in designing and performing the impact experiments, Remi Lansiaux, Wang Wei and Bader Altoaimi for performing initial studies, Hugo De Vuyst for the help with the instrumentation and Cranfield University (UK) for enabling a part of this work to be performed.

References

[1] Gupta NK, Iqbal MA and Sekhon GS. Effect of projectile nose shape, impact velocity and target thickness on the deformation behavior of layered plates *Int. J. Impact Eng.* 2008; 35(1): 37-60.

[2] Gupta NK, Iqbal MA and Sekhon GS. Effect of projectile nose shape, impact velocity and target thickness on deformation behavior of aluminum plates *Int. J. Solids Struct.* 2007; 44(10): 3411-3439.

[3] Arias A, Rodríguez-Martínez JA and Rusinek A. Numerical simulations of impact behaviour of thin steel plates subjected to cylindrical, conical and hemispherical non-deformable projectiles *Eng. Fract. Mech.* 2008; 75(6): 1635-1656.

[4] Jankowiak T, Rusinek A and Wood P. A numerical analysis of the dynamic behaviour of sheet steel perforated by a conical projectile under ballistic conditions, *Finite Elem. Anal. Des.* 2013; 65: 39-49.

[5] Rusinek A, Rodríguez-Martínez, JA, Arias A, et al. Influence of conical projectile diameter on perpendicular impact of thin steel plate *Eng. Fract. Mech.* 2008; 75(10): 2946-2967.

[6] Rodríguez-Millán M, Vaz-Romero A, Rusinek A, et al. Experimental Study on the Perforation Process of 5754-H111 and 6082-T6 Aluminium Plates Subjected to Normal Impact by Conical, Hemispherical and Blunt Projectiles *Exp. Mech.* 2014; 54(5): 729-742.

[7] Børvik T, Hopperstad OS and Pedersen KO. Quasi-brittle fracture during structural impact of AA7075-T651 aluminium plates *Int. J. Impact Eng.* 2010; 37(5): 537-551.

[8] Erice B, Pérez-Martín MJ, Gálvez F. An experimental and numerical study of ductile failure under quasi-static and impact loadings of Inconel 718 nickel-base superalloy *Int. J. Impact Eng.* 2014; 69: 11-24.

[9] Jordan JB and Naito CJ. An experimental investigation of the effect of nose shape on fragments penetrating GFRP *Int. J. Impact Eng.* 2014; 63: 63-71.

[10] Ulven C, Vaidya UK and Hosur MV. Effect of projectile shape during ballistic perforation of VARTM carbon/epoxy composite panels *Compos. Struct.* 2003; 61(1-2): 143-150.

[11] Tan VBC, Lim CT and Cheong CH. Perforation of high-strength fabric by projectiles of different geometry *Int. J. Impact Eng.* 2003; 28(2): 207-222.

[12] Wang J and Zhou N. Damage mechanism and anti-penetration performance of explosively welded plates impacted by projectiles with different shapes *Mater. Des.* 2013; 49: 966-973.

[13] Wang X and Shi J. Validation of Johnson-Cook plasticity and damage model using impact experiment *Int. J. Impact Eng.* 2013; 60: 67-75

[14] Buyuk M, Loikkanen M and Kan CD. Explicit Finite Element Analysis of 2024-T3/T351 Aluminum Material Under Impact *Loading for Airplane Engine Containment and Fragment Shielding*, Report for U.S. Department of Transportation Federal Aviation Administration, Report no. DOT/FAA/AR-08/36, September 2008. FAA.

[15] Kelly S and Johnson G. *Statistical Testing of Aircraft Materials for Transport Airplane Rotor Burst Fragment Shielding*, Report for U.S. Department of Transportation Federal Aviation Administration, Report no. DOT/FAA/AR-06/9, May 2006.

[16] Kay G, Goto D and Couch R. *Statistical Testing and Material Model Characterisation of Aluminum and Titanium for Transport Airplane Rotor Burst Fragment Shielding*, Report for U.S. Department of Transportation Federal Aviation Administration, Report no. DOT/FAA/AR-07/26, August 2007.

[17] Ryabov AA, Romanov VI, Kukanov SS, et al. Numerical Simulation of Elastic-Plastic Deformation of Aircraft Fuel Tank Access Cover Impacted by Tyre Fragment. In *9th European LS-Dyna Conference* Manchester, UK, 2-4 June 2013, ARUP.

[18] Williamsen JE, Schonberg WP, Evans H, et al. A comparison of NASA, DoD, and hydrocode ballistic limit predictions for spherical and non-spherical shapes versus dual- and single-wall targets, and their effects on orbital debris penetration risk, *Int. J. Impact Eng.* 2008; 35(12): 1870-1877.

[19] European Aviation Safety Agency. *Certification Specifications for Large Aeroplanes*, Report for European Aviation Safety Agency, Report no. CS-25, (From Amendment 3, 19 September 2007) Section AMC 25.963(e)

[20] Børvik T, Dey S and Clausen AH. Perforation resistance of five different high-strength steel plates subjected to small-arms projectiles *Int. J. Impact Eng.* 2009; 36(7): 948-964.

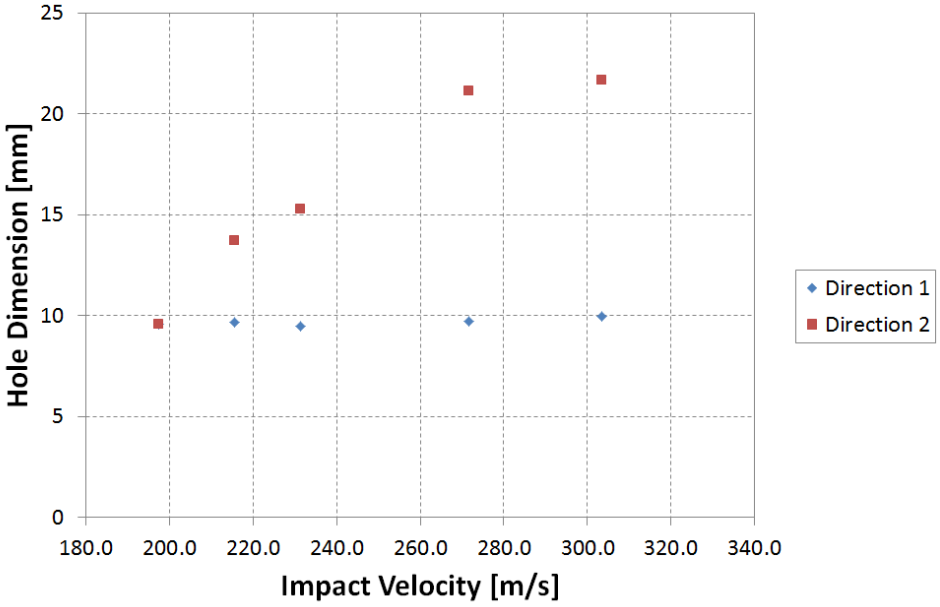

(a)

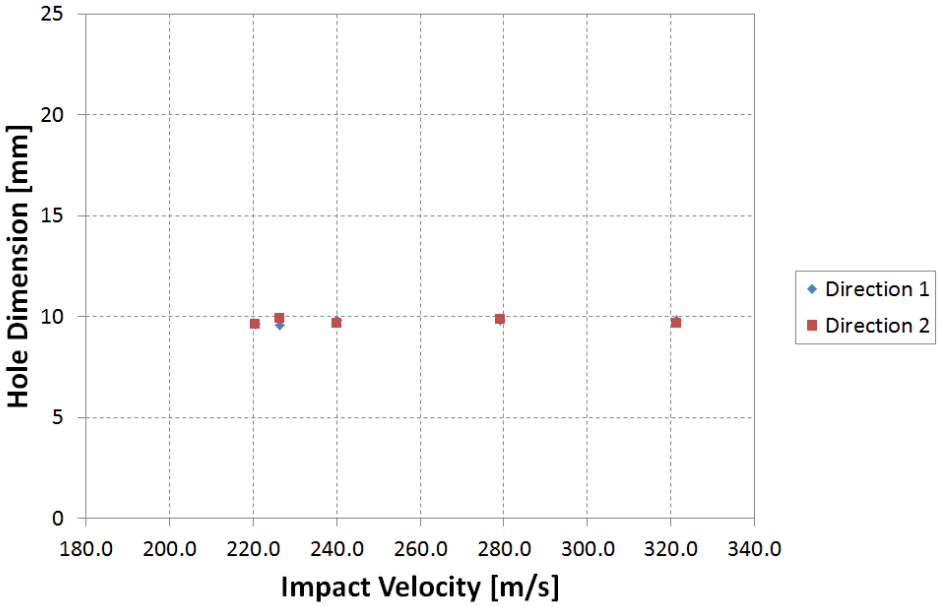

(b)

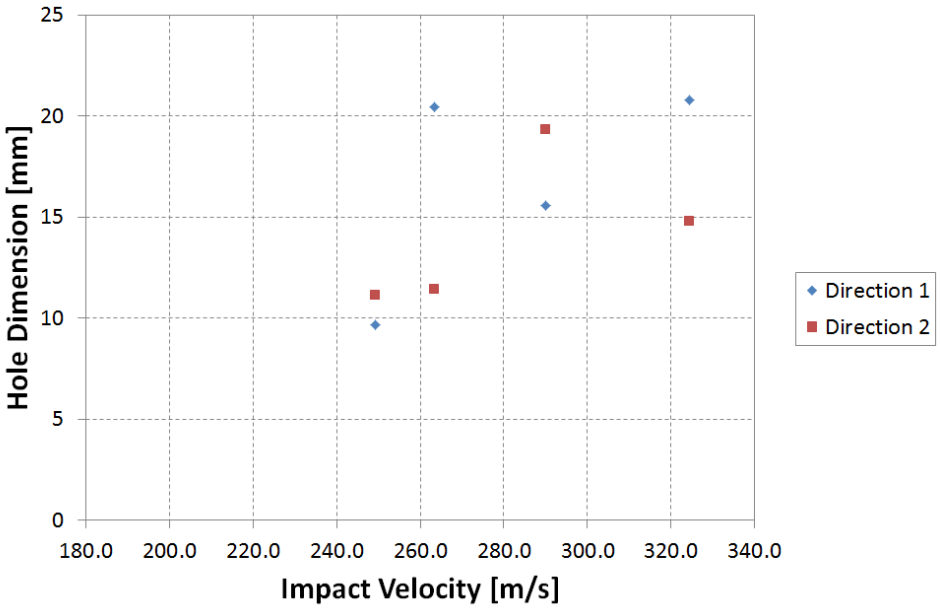

(c)

Fig. 6. Variation of hole diameter with impact velocity for a) edge, b) face and c) corner impact. Direction 1 is perpendicular to clamped

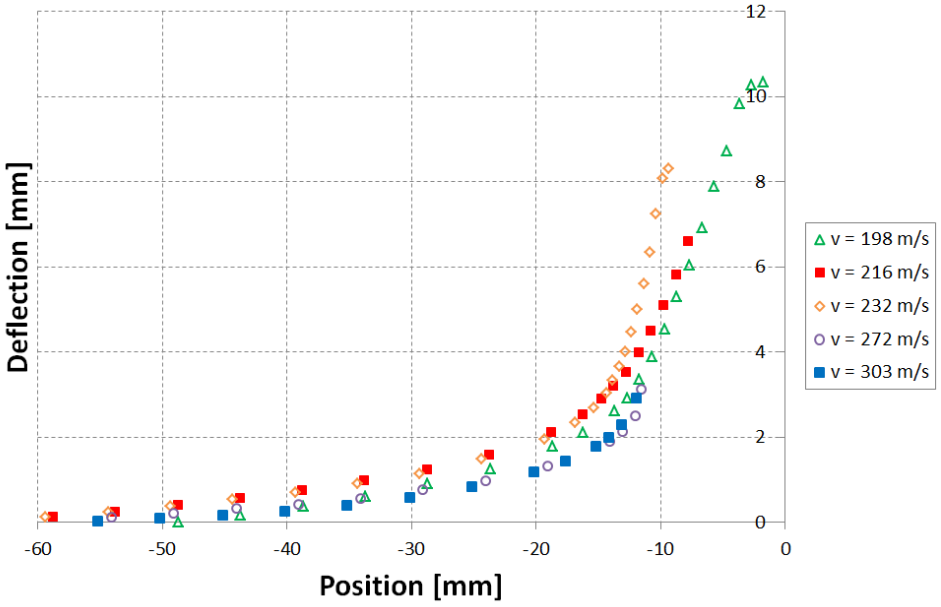

(a)

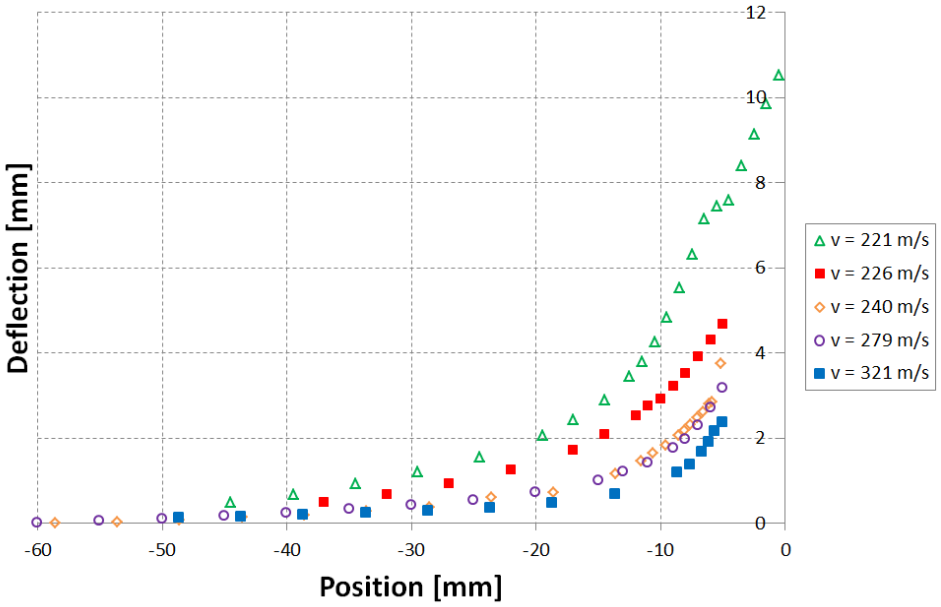

(b)

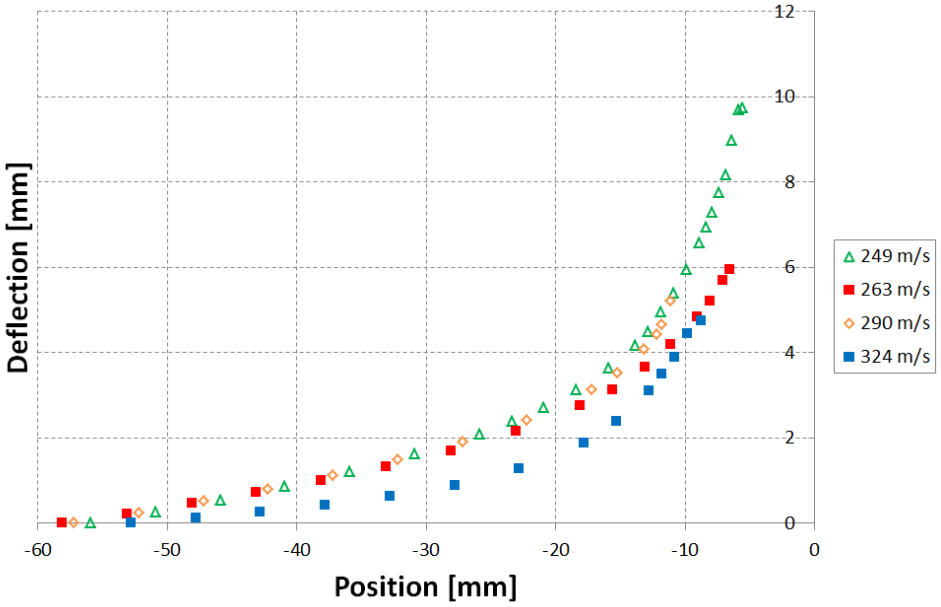

(c)

Fig. 7. Dishing of targets in the case of a) edge; b) face; c) corner impact configuration